EASR

Engineering and Applied Science Research

https://www.tci-thaijo.org/index.php/easr/index

Published by the Faculty of Engineering, Khon Kaen University, Thailand

Turbulent flow and heat transfer behaviors in a circular tube fitted with multiple V–baffles

Teerapat Chompookham[1)], Pongjet Promvonge[2)], Sompol Skullong[3)], Narin Siriwan[1)], Bopit Bubphachot[1)], Kittinan Wansasueb[4)] and Pitak Promthaisong*[1)]

[1)]Heat Pipe and Thermal Tool Design Research Unit (HTDR), Faculty of Engineering, Mahasarakham University, Maha Sarakham 44150, Thailand
[2)]Department of Mechanical Engineering, School of Engineering, King Mongkut's Institute of Technology Ladkrabang, Bangkok 10520, Thailand
[3)]Energy Systems Research Group and ATAE Research Unit, Department of Mechanical Engineering, Faculty of Engineering at Sriracha, Kasetsart University Sriracha Campus, Chonburi 20230, Thailand
[4)]Electronics for Agriculture Research Unit, Faculty of Engineering, Mahasarakham University, Maha Sarakham 44150, Thailand

Received 15 December 2022
Revised 30 March 2023
Accepted 12 April 2023

Abstract

This article presents turbulent flow patterns and thermal behaviors in a circular tube mounted with 30° multiple V–baffles. The influences of V–baffle numbers (*N*) of 2, 3 and 4 with pitch ratios (*PR*) of 1.0, 1.5 and 2.0 for Reynolds number (*Re*) between 3000 and 20,000 were investigated numerically at a fixed blockage ratio, *BR* = 0.05. These simulated results were proposed in four sections: numerical validations, flow and thermal characteristics and thermal performance. It was visible that the multiple V–baffles can help induce the impinging jet leading to disrupting the boundary layer, increasing the fluid mixing, and then enhancing the heat transfer above the plain tube alone. The rises of the number of V–baffles and the lower baffle pitch length led to raising the heat transfer and friction loss. The maximum thermal performance was obtained around 2.06 at *N* = 4, *PR* = 1.0 and lower *Re*.

Keywords: Multiple V–baffle, Turbulent flow, Heat transfer, Circular tube

Nomenclature

A	surface area of tube, m^2	Re	Reynolds number, (-)
BR	blockade ratio, (-)	S	rate of mean strain, s^{-1}
B	baffle height, m	S_ε	source term of ε, kg m^{-1} s^{-4}
C_1	turbulence model coefficient, (-)	S_k	source term of k, kg m^{-1} s^{-3}
C_2, $C_{1\varepsilon}$	turbulence model constant, (-)	S_{ij}	rate of mean strain tensor, s^{-1}
$C_{3\varepsilon}$	degree of ε by buoyancy, (-)	TEF	thermal enhancement factor, (-)
D	tube diameter, m	T	temperature, K
F	friction factor, (-)	u_0	average fluid velocity, m s^{-1}
G_k	turbulence kinetic energy production from mean velocity gradients, kg s^{-3} m^{-1}	u_i	velocity component in x_i-direction, m s^{-1}
G_b	turbulence kinetic energy production from buoyancy, kg s^{-3}	$u_1^{'}$	fluctuation velocity in x_i-direction, m s^{-1}
K	turbulence kinetic energy, m^2 s^{-2}	u_j	velocity component in x_j-direction, m s^{-1}
N	number of baffle, (-)	$u_j^{'}$	fluctuation velocity in x_j-direction, m s^{-1}
Nu	Nusselt number, (-)	u_k	velocity component in x_k-direction, m s^{-1}
Nu_x	local Nusselt number, (-)	x_i, x_j	coordinate direction, m
P	pressure, Pa	x	x-position, m
PR	baffle pitch ratio, (-)	y	y-position, m
Pr	Prandtl number, (-)	z	z-position, m
p	baffle pitch length, m	y^+	distance between first near–wall cell center and duct surface, (-)

Greek letters

ρ	density, kg m^{-3}	η	ratio of turbulence to mean strain, (-)
α	attack angle, degree	Γ_t	turbulent/eddy thermal diffusivity, kg s^{-1} m^{-1}
δ_{ij}	Kronecker delta, m	Γ	molecular thermal diffusivity, kg s^{-1} m^{-1}
σ_k	turbulent Prandtl numbers of k, (-)	ε	rate of turbulence dissipation, m^2 s^{-3}
σ_ε	turbulent Prandtl numbers of ε, (-)	μ	dynamic viscosity, kg s^{-1} m^{-1}

*Corresponding author.
Email address: pitak.p@msu.ac.th
doi: 10.14456/easr.2023.28

Subscripts

0	plain tube
a	air
t	turbulent

Superscript

—	average

1. Introduction

The heat transfer augmentation in a heating/cooling system with the passive technique have been widely utilized in several engineering applications such as a shell–tube heat exchanger, cooling of electronic devices and thermal regenerator to promote the convection coefficient in those system leading to reducing cost, weight, and size of such a system. There have been many attempts to augment heat transfer in a heat exchanger tube by employing diverse vortex generators (VGs) such as ribs, baffles, winglets, and twisted tapes to change the main flow behaviors like swirl flow, reattachment flow, impinging jet flow and counter–rotation vortex flow. These phenomena result in disturbing the boundary layer, rising fluid mixing, and increasing the rate of heat transfer and efficiency.

Promvonge et al. [1] introduced the impact of angled rings on the enhanced heat transfer of a round tube using the ring inserts with blockage ratios of 0.1–0.2 and pitch ratios of 0.5–2.0 at an angle of attack of 30º. They found that the rings provide greater heat transfer and friction loss than the plain tube alone. The *TEF* around 1.0–1.4 was achieved. In addition, Promvonge et al. [2] explored the employ of inclined horseshoe baffles inserted in a heat exchanger tube for baffle blockage ratios of 0.1–0.2 and pitch ratios of 0.5–2.0 at one attack angle of 20º. They found that the horseshoe baffles help increase the rate of heat transfer around 32–208% over the plain tube, leading to the *TEF* in a range of 1.34–1.92. Also, the application of 30° oblique horseshoe baffles to enhance heat transfer inside a duct was experimentally and numerically explored by Skullong et al. [3] who reported that the greatest *TEF* was found at *BR* = 0.2 and *PR* = 1.0. Skullong et al. [4] studied the effect of staggered–winglet perforated–tapes (WPT) inserted in a circular tube on heat transfer enhancement by using the winglet blockage ratios of 0.1–0.3 and pitch ratios of 0.5–1.5 at a single attack angle of 30º. They reported that *TEF* is obtained around 1.2–1.71 and has a maximum for the tape with *PR*=1.0. The influence of quadruple perforated–delta–winglet pairs (PW–XT) on heat transfer enhancement in a tube was examined by Skullong et al. [5] by utilizing the PW–XT with *BR* = 0.10 – 0.25, *PR* = 0.5–2.0 at a fixed attack angle of 30º and reported that increasing *BR* and decreasing *PR* led to the rise in the friction loss and Nusselt number. The maximum *TEF* at *PR* = 1.0 was approximately 1.9. Chingtuaythong et al. [6] explored the heat transfer augmentation in a circular tube inserted with V–shaped rings having *BR* = 0.1–0.2 and *PR* = 0.5–2.0 at a single angle of attack of 30º and proposed that the V–shaped rings can increase the heat transfer around 5.8 times above the plain tube. The *TEF* was around 1.36–1.63 and its maximum was at *PR* = 1.0. Xu et al. [7] examined numerically the thermal performance of a circular tube inserted with winglet vortex generators and found that the swirling flows created by the winglets help increase fluid mixing and enhance the heat transfer. The *TEF* was about 1.03–1.3. Chamoli et al. [8] studied the heat transfer enhancement in a circular tube fitted with perforated vortex generators (PVGs) and reported that there are flow recirculation and jet flow reattachment created by the PVGs and the pair counter–rotation vortex flows appeared at the cross–sectional plane help promote the convection coefficient of the tube surface. The *TEF* was up to 1.13–1.65. Liu et al. [9] investigated the laminar flow and thermal characteristics in a round tube with multiple conical strips that create the multiple longitudinal vortices along the tube resulting in the friction factor, heat transfer, and *TEF* greater than the plain tube around 2.40–28.74, 2.54–7.63, and 1.23–6.05, respectively. Wang et al. [10] suggested the employ of streamwise vortex generators to rise the heat transfer in the tube wall. Liang et al. [11] examined the effect of inclination angles (α = 0–30º) and attack angle (β = 0–45º) of the winglet vortex generator insert on thermal performance of a round tube and suggested that using the winglets leads to the rise of *TEF* around 0.94–1.08. Skullong et al. [12] studied the effect of the curved–winglet tapes (CWT) with *BR* = 0.1–0.3, *PR* = 0.5–2.0 at a fixed angle of attack of 45º on the performance improvement of a circular tube and reported that the CWT produces longitudinal counter–rotating vortices along the tube and helps destroy the boundary layer resulting in a greater rise of heat transfer. The *TEF* of the CWT insert was around 1.34–1.76. Zhai et al. [13] explored the use of winglet-type vortex generator pairs to rise the heat transfer and found that *TEF* around 1.0–1.44 can be achieved. Promvonge and Skullong [14, 15] investigated the V–baffle inserts in a circular tube and proposed that the V–baffle can generate two pairs of counter–rotation vortices leading to multiple impingement–jets on the tube wall to enhance the convection coefficient. Changcharoen et al. [16] offered that the regularly spaced overlap dual twisted tape generated the swirl flow around the tube wall leading to enhancing the heat transfer. The effect of diamond-shaped rings in the circular tube on thermal performance was investigated by Promthaisong and Skullong [17]. They reported that the diamond-shaped rings can increase the *TEF* at around 1.57. Hoonpong et al. [18] reported that the 45º inclined perforated rings generated the vortex flow through the tube and help to rise the turbulence intensity, the heat transfer increased around 236–338% above the plain tube. Lamlerd et al. [19] found that the circular ring in the steam generator can up the heat transfer around 6.88–10.35%. The use of circular-rings combined with the twisted tape was investigated by Pimsarn et al. [20]. They suggested that the inclined rings give the greater heat transfer than the transverse arrangement. The thermal performance of the tube with louvered winglet tapes and louvered corner-curved winglet tapes were reported by Promvonge and Skullong [21] as well as Jayranaiwachira et al. [22], respectively. They reported that the winglet tapes investigated greater augmentation in both heat transfer and pressure loss. In addition, the counter–rotating vortices and multiple vortices flow were also generated by the vortex-flow corrugated tube and cross corrugated tube [23]. The strong vortex strength increased led to the increase in heat transfer. Moreover, the effects of swirl flow devices in a tube on heat transfer augmentation have been investigated such as the decreased tapered twisted tapes [24], twisted trapezoidal tapes [25], sawtooth twisted tapes [26], twisted wavy tapes [27] and triple-blade vortex generator [28]. In general, the swirl flow will be created along the tube. The flow strength and the mixing between the core fluid and the near tube wall fluid region increased led to the rise in the heat transfer. However, the twisted tapes mounted at the core flow provided a larger pressure drop due to main flow blockage. This is the reason that the overall thermal performance is limited.

From the above literature, it indicates that *TEF* of the V–shaped baffle is superior to that of other turbulators. It is because the V–baffles produce the pair–counter–rotating vortices leading to the boundary layer disruption and fast fluid mixing better than the others. However, the V–baffles mounted at the core flow cause a higher pressure drop due to main flow blockage, higher pumping power loss. In this paper, the V–baffle is mounted at the tube wall to avoid disturbing the core flow and to reduce the higher pressure drop. The multiple V–baffles are designed to increase the wall area of impinging–jets.

2. Mathematical foundation

The turbulent flow structure and thermal patterns inside a round tube fitted with multiple V–baffles were described via the governing equations with the following assumptions: steady state, three–dimensional incompressible flow and ignoring the radiation heat transfer. The governing equations [29] are written by:

Continuity equation:

$$\frac{\partial(\rho u_{\mathrm{i}})}{\partial x_{\mathrm{i}}}=0 \tag{1}$$

Momentum equations:

$$\frac{\partial(\rho u_{\mathrm{i}} u_{\mathrm{j}})}{\partial x_{\mathrm{j}}}=-\frac{\partial P}{\partial x_{\mathrm{i}}}+\frac{\partial}{\partial x_{\mathrm{j}}}\left[\mu\left(\frac{\partial u_{\mathrm{i}}}{\partial x_{\mathrm{j}}}-\rho\overline{u_{\mathrm{i}}' u_{\mathrm{j}}'}\right)\right] \tag{2}$$

where $-\rho\overline{u_i' u_{\mathrm{j}}'}$ is the Reynolds stresses and given as:

$$-\rho\overline{u_{\mathrm{i}}' u_{\mathrm{j}}'}=\mu_{\mathrm{t}}\left(\frac{\partial u_{\mathrm{i}}}{\partial x_{\mathrm{j}}}+\frac{\partial u_{\mathrm{j}}}{\partial x_{\mathrm{i}}}\right)-\frac{2}{3}\left(\rho k+\mu_{\mathrm{t}}\frac{\partial u_{\mathrm{k}}}{\partial x_{\mathrm{k}}}\right)\delta_{\mathrm{ij}} \tag{3}$$

Energy equation:

$$\frac{\partial(\rho u_{\mathrm{i}} T)}{\partial x_{\mathrm{i}}}=\frac{\partial}{\partial x_{\mathrm{j}}}\left[(\Gamma+\Gamma_{\mathrm{t}})\frac{\partial T}{\partial x_{\mathrm{j}}}\right] \tag{4}$$

For turbulent region, the Realizable *k*–*ε* turbulence model [30] is adopted in the computation domain. The *k* and ε equations are expressed in Eqs. (5) and (6), respectively.

$$\frac{\partial(\rho k)}{\partial t}+\frac{\partial(\rho k u_{\mathrm{j}})}{\partial x_{\mathrm{j}}}=\frac{\partial}{\partial x_{\mathrm{j}}}\left[\left(\mu+\frac{\mu_{\mathrm{t}}}{\sigma_{\mathrm{k}}}\right)\frac{\partial k}{\partial x_{\mathrm{j}}}\right]+G_{\mathrm{k}}+G_{\mathrm{b}}-\rho\varepsilon+S_{\mathrm{k}} \tag{5}$$

and

$$\frac{\partial(\rho\varepsilon)}{\partial t}+\frac{\partial(\rho\varepsilon u_{\mathrm{j}})}{\partial x_{\mathrm{j}}}=\frac{\partial}{\partial x_{\mathrm{j}}}\left[\left(\mu+\frac{\mu_{\mathrm{t}}}{\sigma_{\varepsilon}}\right)\frac{\partial\varepsilon}{\partial x_{\mathrm{j}}}\right]+\rho C_1 S_{\varepsilon}-\rho C_2\frac{\varepsilon^2}{k+\sqrt{\nu\varepsilon}}+C_{1\varepsilon}\frac{\varepsilon}{k}C_{3\varepsilon}G_{\mathrm{b}}+S_{\varepsilon} \tag{6}$$

where

$$C_1=\max\left[0.43,\frac{\eta}{\eta+5}\right],\ \eta=S\frac{k}{\varepsilon},\ S=\sqrt{2S_{\mathrm{ij}}S_{\mathrm{ij}}},\ S_{\mathrm{ij}}=\frac{1}{2}\left(\frac{\partial u_{\mathrm{j}}}{\partial x_{\mathrm{i}}}+\frac{\partial u_{\mathrm{i}}}{\partial x_{\mathrm{j}}}\right) \tag{7}$$

The constants appearing in the equations are provided as follows:

$$\sigma_{\mathrm{k}}=1.0,\ \sigma_{\varepsilon}=1.2,\ C_{1\varepsilon}=1.44,\ C_2=1.9 \tag{8}$$

In the current computation, the finite volume method [31] with the SIMPLE algorithm and the QUICK scheme are used to solve the problem. The normalized residual values for the equation of energy are to be converged at below 10^{-9} while the ones for other equations are converged at lower 10^{-5}.

Four parameters of interest, the Reynold number (*Re*), average Nusselt number (*Nu*), friction factor (*f*), as well as thermal enhancement factor (*TEF*), are evaluated for the tube fitted with multiple V–baffles below.

The Reynolds number:

$$Re=\rho u_0 D/\mu \tag{9}$$

The friction factor:

$$f=(-dP/dx)D/(1/2)\rho u_0^2 \tag{10}$$

The average Nusselt number:

$$Nu = \frac{1}{A}\int Nu_x dA \tag{11}$$

Here, $Nu_x = \frac{q'' D}{k_a\left(T_w(x) - T_{bm}\right)}$, where T_w is the wall temperature, T_{bm} is the local bulk mean air temperature obtained by linearly interpolating the T_{bm} at the outlet and inlet, while q'' is the wall heat flux.

The thermal enhancement factor:

$$TEF = \left(Nu / Nu_0\right)/\left(f / f_0\right)^{1/3} \tag{12}$$

where u_0 is the average fluid velocity, while f_0 and Nu_0 stand for the friction factor and the average Nusselt number, respectively, for the plain tube.

3. Physical models and boundary conditions

The geometric configuration of the test tube was carried out using the circular tube fitted with multiple V–baffles as depicted in Figure 1. The parameter values for the multiple V–baffles, the blockage ratio, $BR = b/D = 0.05$, angle of attack, $\alpha = 30^o$, were set to constant. A number of multiple V–baffles, $N = 2$, 3 and 4 and pitch ratio, $PR = p/D = 1.0$, 1.5 and 2.0 were varied.

The hexahedron elements were applied to all grids of the computational domain where a high–density grid ($y^+ \approx 1$) was set near the tube wall because the temperature and velocity fields were significant altered owing to the fluid viscosity. The grid numbers for the computational domain used around 523,800 elements because increasing the number of elements from 523,800 to 752,600 changed the friction factor and Nusselt number under 0.5%, while the increase in the element number from 251,600 to 523,800 results in a significant change in the friction factor and Nusselt number.

The boundary conditions of the computational domain were as follows. (1) the inlet and outlet planes were set to periodic flow conditions, (2) the working fluid was air at 300 K ($Pr = 0.707$) in which the physical properties were assumed to remain constant, (3) the tube wall was set with a uniform 600 W/m^2 heat flux, and (4) all the surface had a no–slip condition.

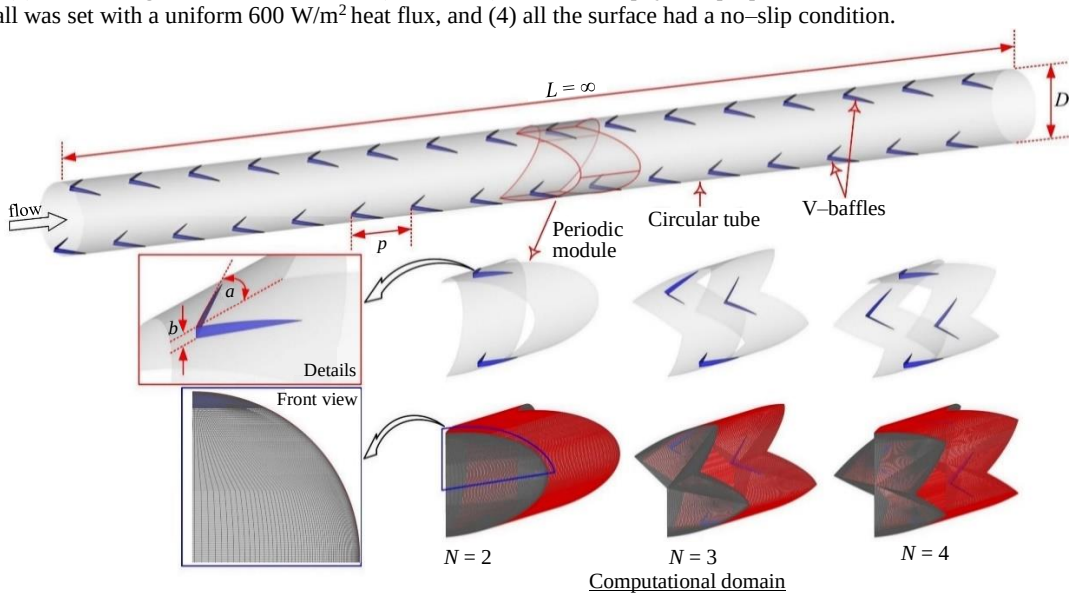

Figure 1 The geometries of a circular tube fitted with multiple V–baffles and computational domain.

4. Results and discussion

4.1 Validation

To validate the accuracy of the numerical results, the Nusselt number and friction factor of the plain tube by using four turbulent models, SST k–ω, Realizable k–ε, RNG k–ε and standard k–ε models were compared with the standard correlations [31] and experimental data by Chingtuaythong et al. [6] as presented in Figure 2.

The *Nu* correlation of Dittus-Boelter for heating:

$$Nu = 0.023 Re^{0.8} Pr^{0.4} \tag{13}$$

The *f* correlation of Blasius:

$$f = 0.316 Re^{-0.25} \tag{14}$$

In the figure, the Realizable k–ε turbulence model had the results close to both the standard correlations and experimental data, the mean discrepancies of the friction factor and Nusselt number were below 10%. In addition, the Realizable k-ε turbulence model was used to validate with measurements of Chingtuaythong et al. [6] as proposed in Figure 2(b). The tube with V-shaped rings at α = 60º, BR = 0.10, PR = 1.0 and 2.0 was selected for this comparison. At similar conditions, it is disclosed that the Nu and f provided the similar trends. The Realizable k-ε turbulence model provided the mean deviation of the Nusselt number and friction factor less than 8.4% with measured data. Thus, the Realizable k–ε turbulent model was the best choice in the current computation.

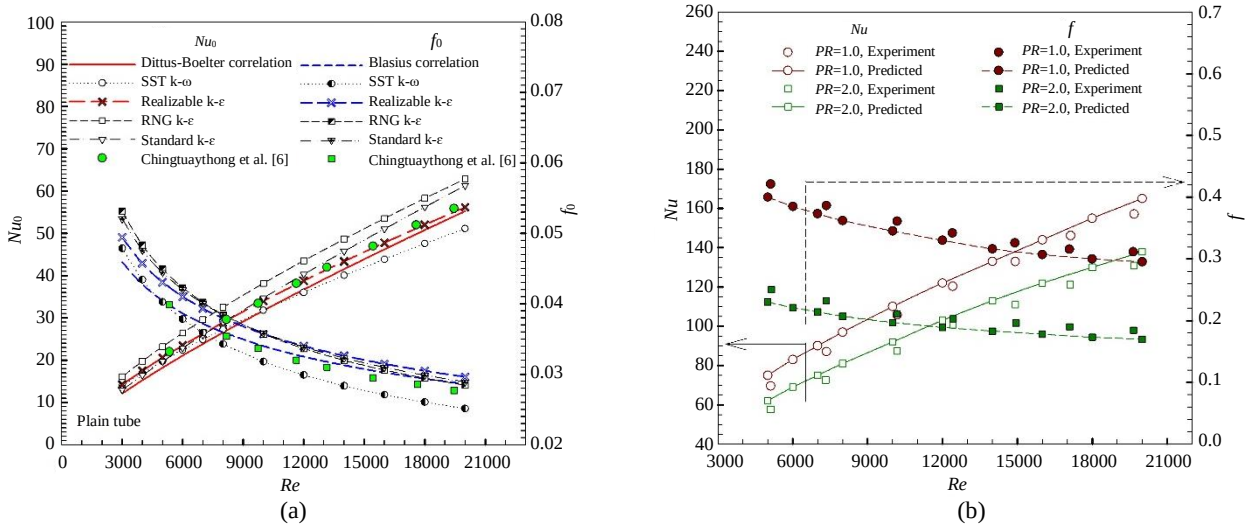

Figure 2 Validations of Nusselt number and friction factor for (a) plain tube and (b) V-ring-inserted tube [6].

4.2 Flow structure and temperature distribution

Figures 3 and 4 show the 3D flow patterns and local wall temperature contours for BR = 0.05, PR = 1.0 and Re = 3000. In general, the multiple V–baffles can generate the streamlines of impingement flows on the tube wall behind the V–baffle region as displayed in Figure 3. As N increases, it increases the streamlines of impinging flows along the tube wall. When considered 3D flow patterns and local wall temperature distributions in Figure 4, the streamlines of impinging flows help disrupt the boundary layer and reduce the wall temperature, especially at the tube wall where the streamlines of impingement flows occur. In the figure, the N = 4 can reduce the wall temperature better than other cases. However, the area where the streamlines of non–impingement–flows attack has high wall temperature.

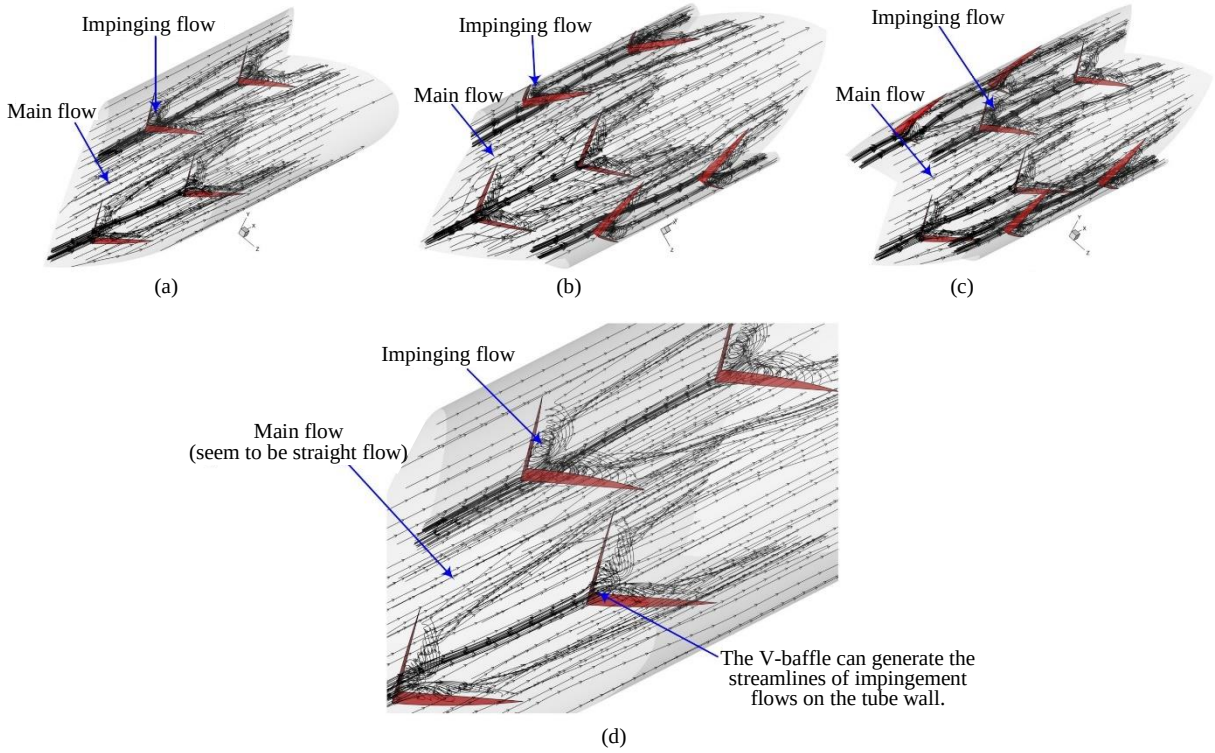

Figure 3 Details of 3D flow patterns for (a) N = 2, (b) N = 3, (c) N = 4 and (d) N = 2 (zoom-in) at PR = 1.0, BR = 0.05, and Re = 3000.

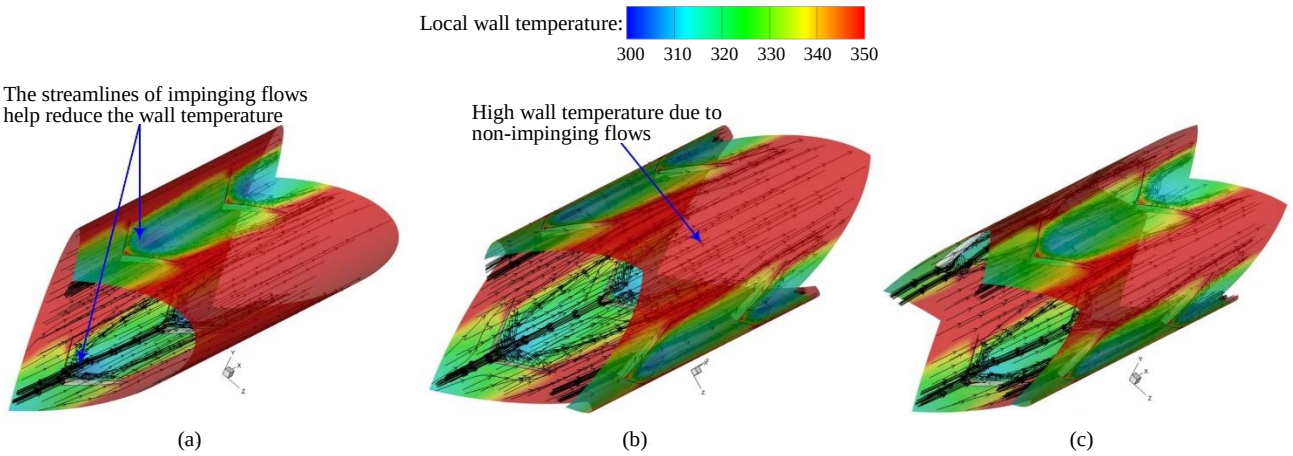

Figure 4 3D local wall temperature contours for (a) N = 2, (b) N = 3 and (c) N = 4 at PR = 1.0, BR = 0.05, and Re = 3000.

Figure 5 depicts the streamline contours in transverse planes for the tube fitted with multiple V–baffles for PR = 1.0, Re = 3000, and BR = 0.05. In general, the multiple V–baffles at N = 2, 3 and 4 can create two, three and four of pair–counter–rotating vortices, respectively. The existence of pair–counter–rotating vortices leads to better mixing of the fluid and helps promote the convection coefficient over the tube wall. In the figure, the increase of N results in higher levels of vortex intensity apart from fast fluid mixing as showed a reduced layer thickness of high fluid temperature near the tube wall. Additionally, the lower temperature fluid at the core was induced to the near tube wall better, especially, at the V–tip region.

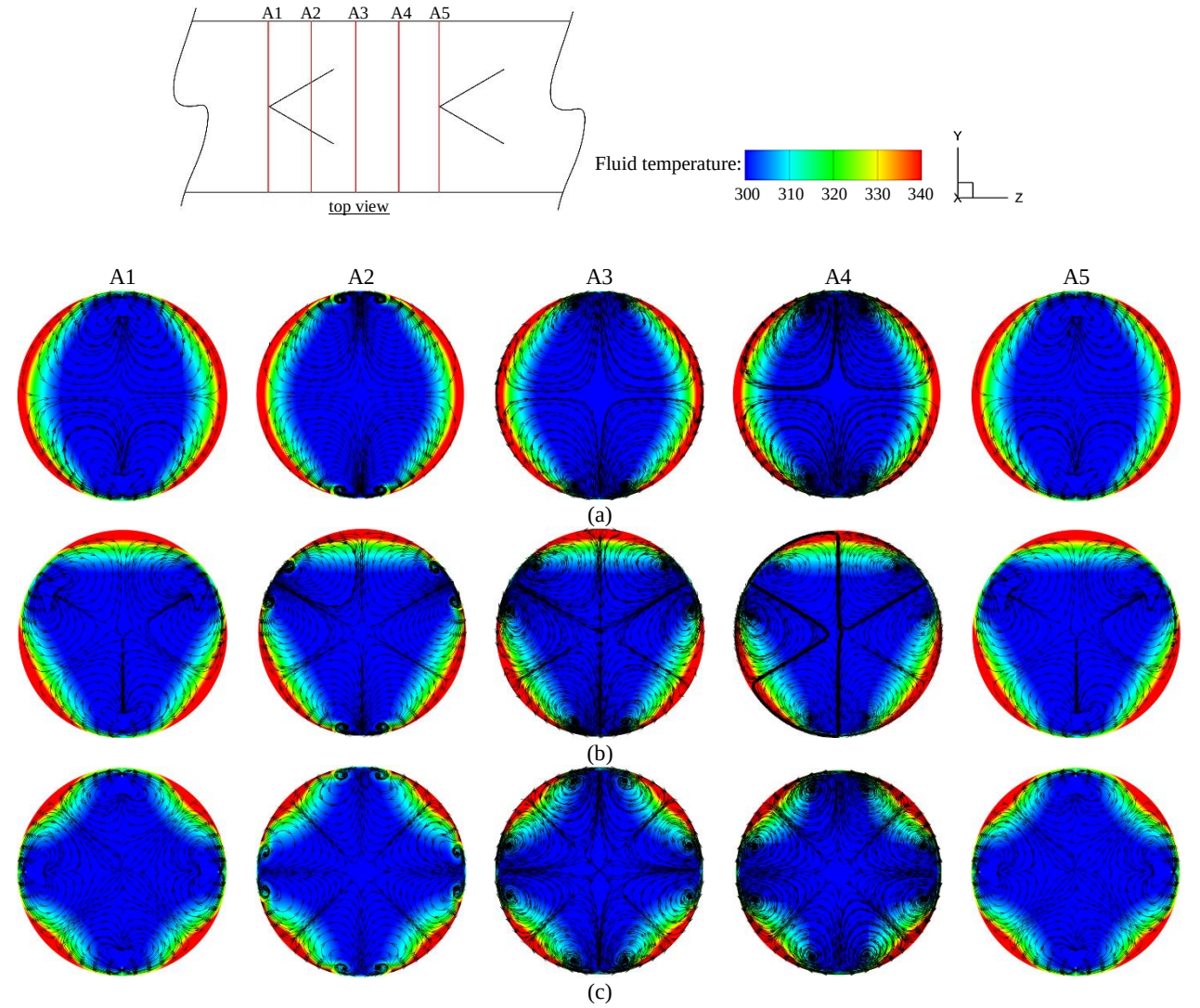

Figure 5 Flow structures and fluid temperature contours in transverse planes for (a) N = 2, (b) N = 3 and (c) N = 4 at PR = 1.0, Re = 3000, and BR = 0.05.

4.3 Heat transfer

The heat transfer characteristics in a tube fitted with multiple V–baffles is presented in terms of local wall Nusselt number contours as depicted in Figure 6. In general, it can be clearly seen that the tube fitted with multiple V–baffles has a higher heat transfer area behind the V–tip where the streamlines of impingement–flows attack. The reason is that the high fluid temperature near the tube wall is reduced leading to increasing the heat transfer between the fluid and the tube wall. Moreover, the counter–rotating vortices help induce the lower fluid temperature at the core to the near wall region. However, the area where the streamlines of non–impingement–flows attack has lower heat transfer. This leads to lower heat transfer between the fluid and tube wall and then higher wall temperature. In the figure, the rise of *N* results in increasing the heat transfer on the tube wall due to more streamlines of impinging jets. However, the area where the streamlines of non–impingement–flows appear has poorer heat transfer.

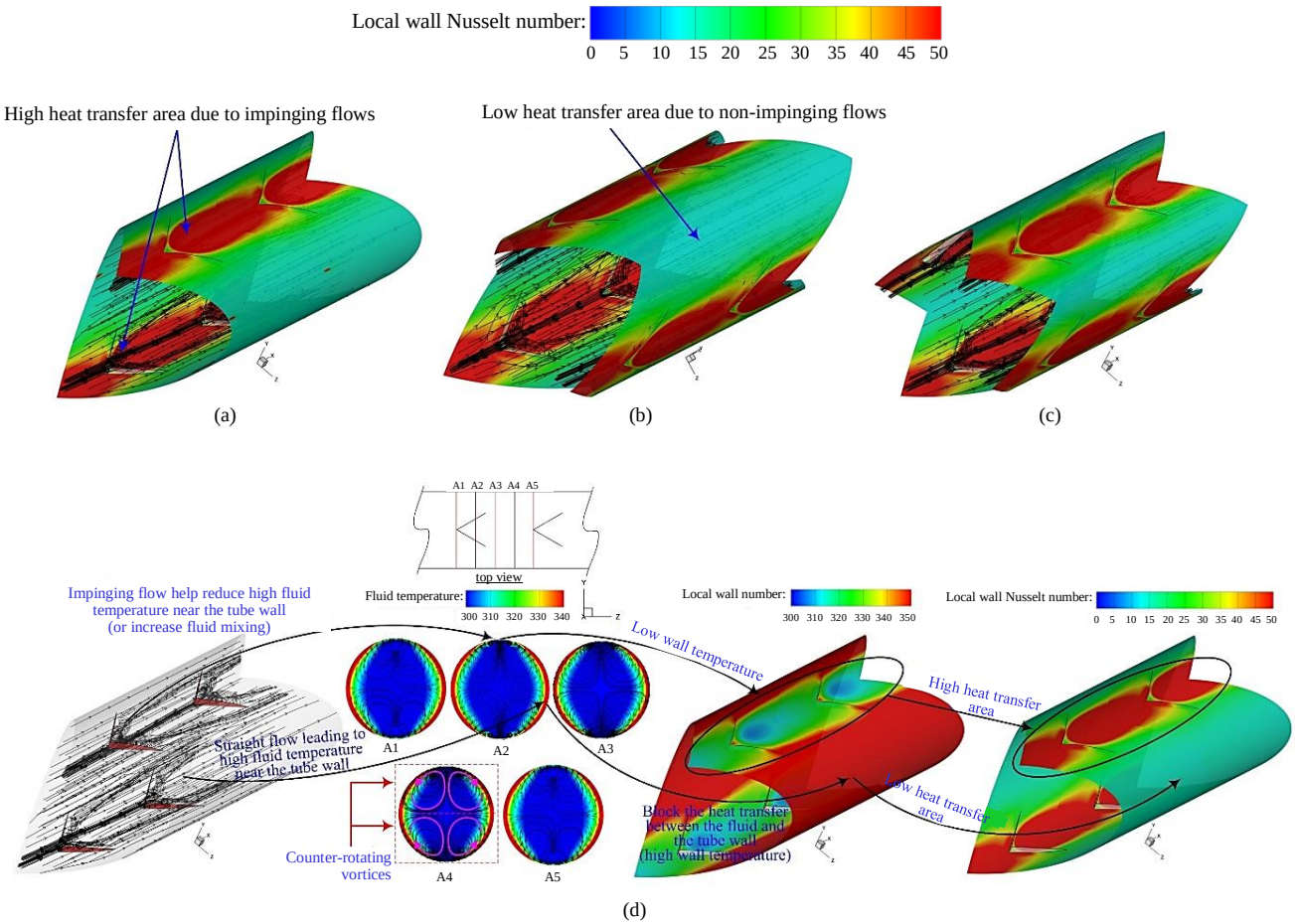

Figure 6 Local Nu contours for (a) N = 2, (b) N = 3, (c) N = 4 and (d) details of flow and heat transfer characteristics for N = 2 at PR = 1.0, Re = 3000, and BR = 0.05.

4.4 Performance evaluation

The variations of Nusselt number ratio (Nu/Nu_0) with Re and N values are presented in Figure 7(a) and (b), respectively. In the figure, Nu/Nu_0 tends to decline with raising Re and PR but has an increasing trend with rising N. The Nu/Nu_0 for all cases investigated is higher than the plain tube alone ($Nu/Nu_0 > 1.0$) owing to faster fluid mixing. In the range investigated, the tube with multiple V–baffles at N = 2, 3 and 4 gives Nu/Nu_0 around 1.05–2.29, 1.13–2.64 and 1.23–2.8 times, respectively. For PR = 1.0, 1.5, and 2.0, the Nu/Nu_0 of N = 4 is greater than that of N = 2 and 3 around 22.15% and 6.19%, 22.4% and 9.31%, and 14.24% and 8.87%, respectively. The maximum Nu/Nu_0 was seen at about 2.8 at N = 4, PR = 1.0 and Re = 3000.

Figures 8(a) and (b) present the variations in the f/f_0 with Re and N values, respectively. It is observed that f/f_0 tends to rise with increasing Re and N but has reversing trend with raising PR values. The f/f_0 values for all cases investigated are higher than the plain tube ($f/f_0 > 1.0$) due to the flow blockage. In the range investigated, the tube with multiple V–baffles at N = 2, 3 and 4 provides f/f_0 in a range of 1.4–2.24, 1.51–2.7 and 1.68–3.18, respectively. The N = 4 provides f/f_0 higher than the N = 2 and 3 at about 41.97% and 17.91%, 27.78% and 13.95%, and 20.38% and 11.64% for PR = 1.0, 1.5, and 2.0, respectively. The greatest f/f_0 is found around 3.18 at PR = 1.0, N = 4, and Re = 20,000.

Figures 9(a) and (b) depict the variations of TEF along with Re and N, respectively. For all cases, TEF obtained at specific friction factor and Nusselt number values are compared at the same pumping power. In the range investigated, TEF values for using multiple V–baffles at N = 2, 3 and 4 are ranging from 0.87–1.9, 0.91–2.05 and 0.95–2.06, respectively. The greatest TEF around 2.06 can be seen at PR = 1.0, N = 4, and Re = 3000.

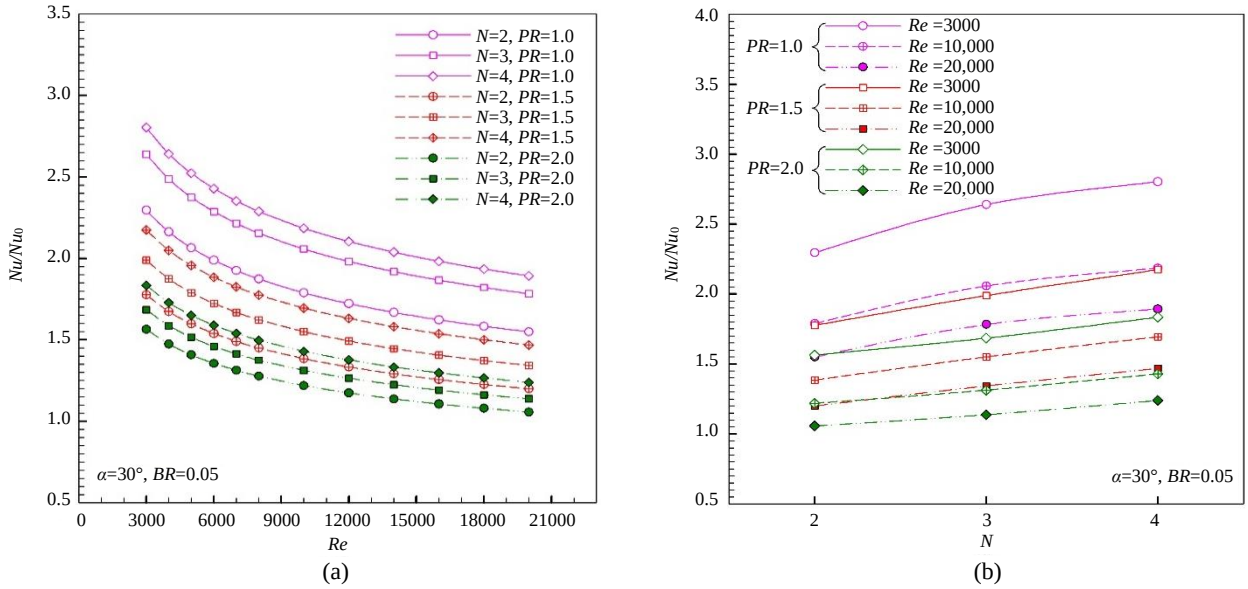

Figure 7 Variations of Nu/Nu_0 with (a) *Re* and (b) *N*.

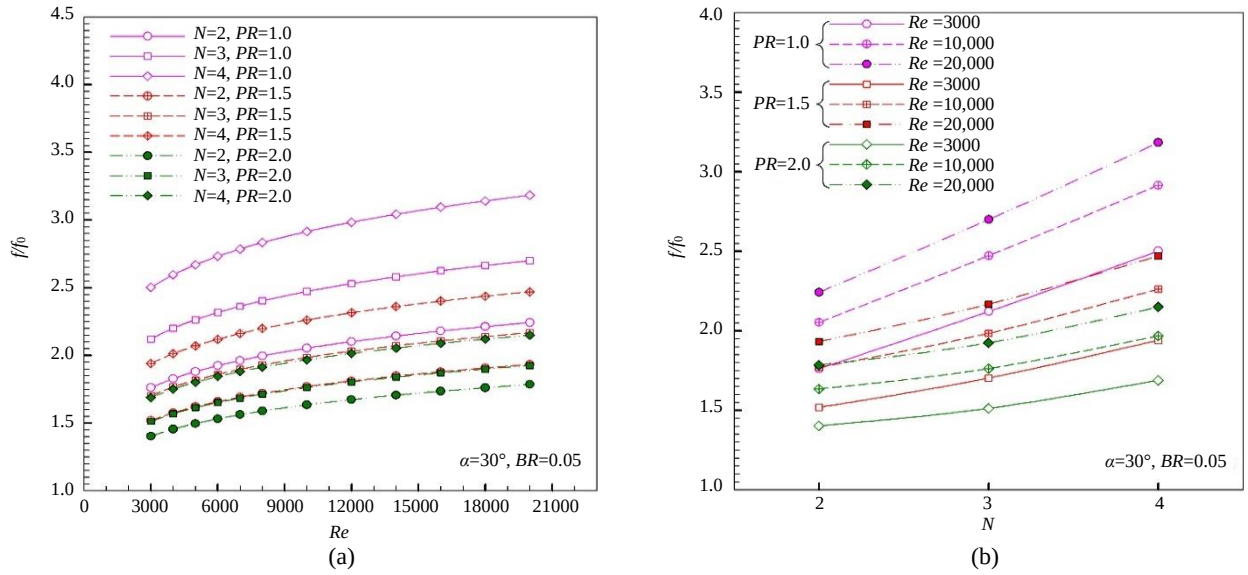

Figure 8 Variations of f/f_0 with (a) *Re* and (b) *N*.

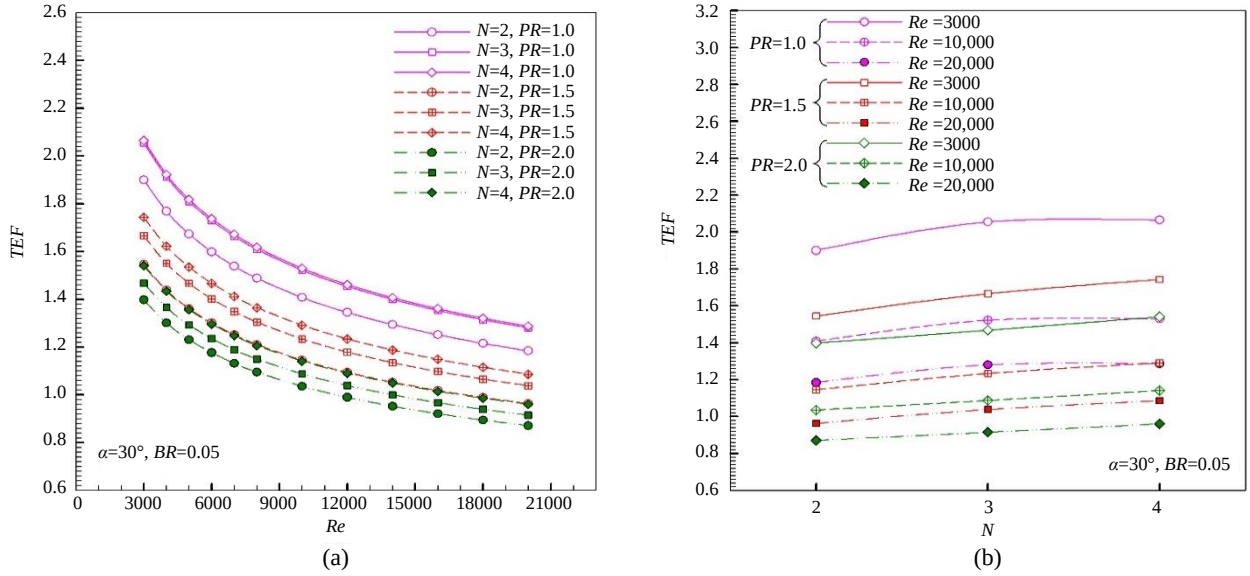

Figure 9 *TEF* variations with (a) *Re* and (b) *N*.

Correlations for the *Nu* and *f* of the 30º multiple V–baffles with constant blockage ratio (*BR* = 0.05) and various pitch ratios (*PR* = 1.0, 1.5 and 3.0), number of multiple V–baffles (*N* = 2, 3 and 4) and Reynolds number (*Re* = 3000-20,000) were written as:

$$Nu = 0.232 Re^{0.593} N^{0.269} PR^{-0.607} Pr^{0.4} \quad (15)$$

$$f = 0.1755 Re^{-0.123} N^{0.371} PR^{-0.465} \quad (16)$$

The plots of the *Nu* and *f* of the 30º multiple V–baffles, predicted by Eqs. (15) - (16) and numerical data are depicted in Figure 10(a) and (b), respectively. In the figure, it is found that the numerical data falls within ±2.8% and ±4.8% for the predicted *Nu* and *f*, respectively.

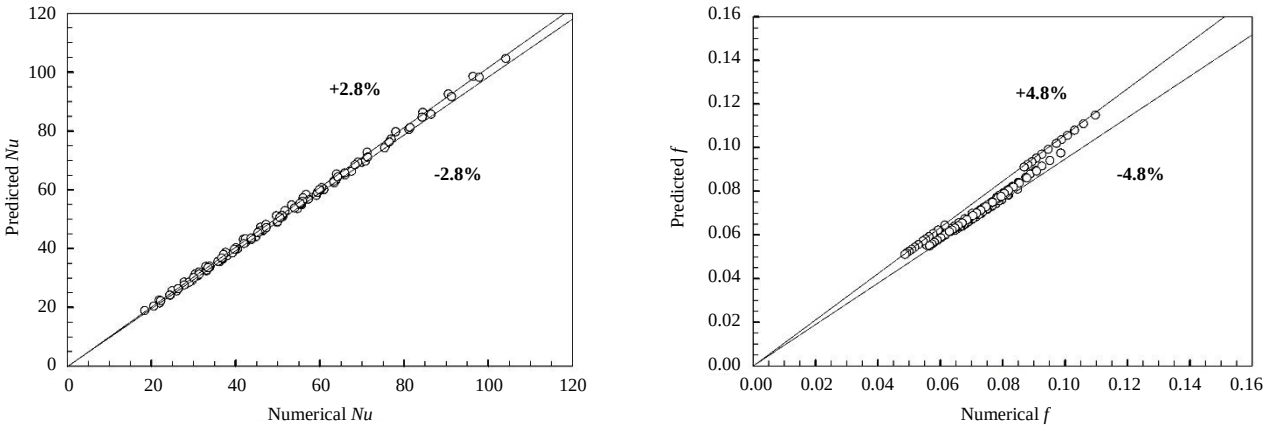

Figure 10 Predicted data of (a) *Nu* and (b) *f* versus numerical data.

5. Comparisons with previous published turbulators

The maximum *TEF* case of the multiple V-baffles (*N* = 4, *PR* = 1.0, *BR* = 0.05, α = 30º) was compared with that of the previous published turbulators, inclined vortex rings (*PR* = 0.5, *BR* = 0.1, α = 30º) [1], horseshoe baffles (P_R = 0.5, B_R = 0.1, α = 20º) [2], staggered-winglet perforated-tapes (P_R = 1.0, B_R = 0.15, α = 30º) [4], quadruple perforated-delta-winglet pairs (P_R = 1.0, B_R = 0.15, α = 30º) [5], v-shaped rings (R_B = 0.1, R_P = 1.0, α = 30º) [6], winglets vortex generator (β = 30º, *BR* = 0.1) [7], perforated vortex generator (p/p_a = 2, *PI* = 16%) [8], v-baffles (R_P = 1.0, R_B = 0.15, α = 30º) [14], v-shaped winglet (R_B = 0.15, R_P = 1.0, α = 45º) [15], diamond-shaped rings (R_B = 0.10, R_P = 1.0, α = 45º) [17], perforated vortex rings (*BR* = 0.1, *PR* = 1.0, α = 45º) [18], twisted trapezoidal tapes (*H* = *w*/4, *T* = 4*D*, *P* = 4/3*D*) [24] and sawtooth twisted tape (*y*/*w* = 3.0, α = 70º) [25] as proposed in Figure 11. In the figure, it was observed that multiple V-baffle provided the mean Nu/Nu_0 higher than ones from [7], [24] and [25] at around 20.83%-63% while lower than others at around 16.95%-92.85%, the mean f/f_0 is higher than that from [7] at around 89% while lower than others at around 12.93%-627.54% and the mean TEF is higher than those from [2], [4], [6-8], [17, 18] and [24, 25] at around 5.21%-44.16% while lower than others at around 7.75%-14.86%. Considering the highest TEF, it was found that the multiple V-baffle has a superior to other turbulators due to lower the friction loss while the familiar *TEF* was presented as V-baffled tapes [14] and V-shaped winglet [15] with values of 2.07 and 2.0, respectively, compared at the lowest Re.

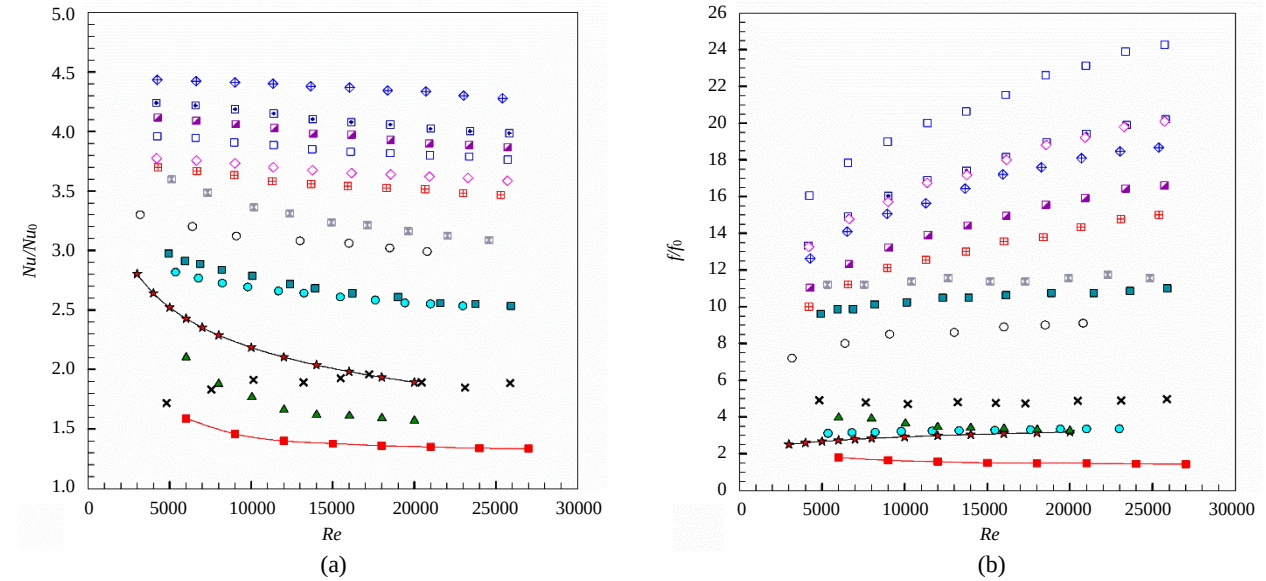

Figure 11 Comparisons with previous VG devices in tubes for (a) Nu/Nu_0, (b) f/f_0 and (c) *TEF* versus *Re*.

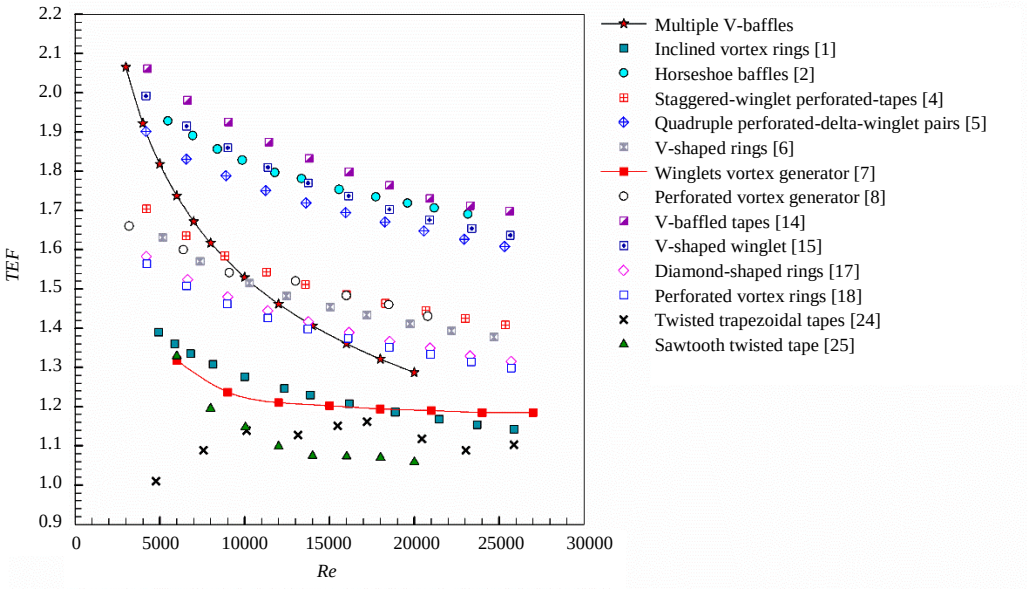

(c)

Figure 11 (continued) Comparisons with previous VG devices in tubes for (a) Nu/Nu_0, (b) f/f_0 and (c) *TEF* versus *Re*.

6. Conclusions

An investigation on thermal behaviors of a turbulent tube flow over the multiple V–baffles has been conducted numerically for *Re* = 3000–20,000. The effect of *N* = 2, 3 and 4 and *PR* = 1.0, 1.5 and 2.0 of the V–baffles at a fixed value of *BR* = 0.05 and α = 30º on *Nu*, *f* and *TEF* characteristics were examined. The major findings include

(1) The streamlines of impinging jets (3D flow structure) and the pair–counter–rotating vortices (in transverse planes) appear for all cases that result in enhancing the heat transfer owing to the fast fluid mixing and higher temperature gradient of fluid near the surface.

(2) The rise of *N* results in raising the friction loss and heat transfer whereas rising *PR* has an opposite trend.

(3) Nu/Nu_0, f/f_0 and *TEF* values for the tube mounted with multiple V–baffles are found in the range of 1.05–2.8, 1.4–3.18 and 0.87–2.06 times, respectively.

(4) The best option for using multiple V–baffle is for *N* = 4, *PR* = 1.0 because at this condition, it has the highest *TEF* around 2.06 at the lowest *Re*. The enhancement of heat transfer mainly comes from the vortices–induced impingement flow or multiple impinging jets created by the V–baffle.

7. Acknowledgements

This Research was Financially Supported by Faculty of Engineering Mahasarakham University.

8. References

[1] Promvonge P, Koolnapadol N, Pimsarn M, Thianpong C. Thermal performance enhancement in a heat exchanger tube fitted with inclined vortex rings. Appl Therm Eng. 2014;62(1):285-92.
[2] Promvonge P, Tamna S, Pimsarn M, Thianpong C. Thermal characterization in a circular tube fitted with inclined horseshoe baffles. Appl Therm Eng. 2015;75:1147-55.
[3] Skullong S, Thianpong C, Jayranaiwachira N, Promvonge P. Experimental and numerical heat transfer investigation in turbulent square-duct flow through oblique horseshoe baffles. Chem Eng Process: Process Intensif. 2016;99:58-71.
[4] Skullong S, Promvonge P, Thianpong C, Pimsarn M. Heat transfer and turbulent flow friction in a round tube with staggered-winglet perforated-tapes. Int J Heat Mass Transf. 2016;95:230-42.
[5] Skullong S, Promvonge P, Thianpong C, Jayranaiwachira N. Thermal behaviors in a round tube equipped with quadruple perforated-delta-winglet pairs. Appl Therm Eng. 2017;155:229-43.
[6] Chingtuaythong W, Promvonge P, Thianpong C, Pimsarn M. Heat transfer characterization in a tubular heat exchanger with V-shaped rings. Appl Therm Eng. 2017;110:1164-71.
[7] Xu Y, Islam MD, Kharoua N. Numerical study of winglets vortex generator effects on thermal performance in a circular pipe. Int J Therm Sci. 2017;112:304-17.
[8] Chamoli S, Lu R, Yu P. Thermal characteristic of a turbulent flow through a circular tube fitted with perforated vortex generator inserts. Appl Therm Eng. 2017;121:1117-34.
[9] Liu P, Zheng N, Shan F, Liu Z, Liu W. An experimental and numerical study on the laminar heat transfer and flow characteristics of a circular tube fitted with multiple conical strips inserts. Int J Heat Mass Transf. 2018;117:691-709.
[10] Wang Y, Liu P, Shan F, Liu Z, Liu W. Effect of longitudinal vortex generator on the heat transfer enhancement of a circular tube. Appl Therm Eng. 2019;148:1018-28.
[11] Liang G, Islam MD, Kharoua N, Simmons R. Numerical study of heat transfer and flow behavior in a circular tube fitted with varying arrays of winglet vortex generators. Int J Therm Sci. 2018;134:54-65.
[12] Skullong S, Promvonge P, Thianpong C, Jayranaiwachira N, Pimsarn M. Thermal performance of heat exchanger tube inserted with curved-winglet tapes. Appl Therm Eng. 2018;129:1197-211.

[13] Zhai C, Islam MD, Simmons R, Barsoum I. Heat transfer augmentation in a circular tube with delta winglet vortex generator pairs. Int J Therm Sci. 2019;140:480-90.
[14] Promvonge P, Skullong S. Augmented heat transfer in tubular heat exchanger fitted with V-baffled tapes. Int J Therm Sci. 2020;155:106429.
[15] Promvonge P, Skullong S. Thermo-hydraulic performance in heat exchanger tube with V- shaped winglet vortex generator. Appl Therm Eng. 2020;164:114424.
[16] Changcharoen W, Somravysin P, Promthaisong P, Eiamsa-ard P, Nanan K, Eiamsa-ard S. Investigation of turbulent heat transfer in round tubes fitted with regularly spaced overlap dual twisted tape elements. J Res Appl Mech Eng. 2015;3(2):64-74.
[17] Promthaisong P, Skullong S. Thermal characterization in circular tube inserted with diamond-shaped rings. J Res Appl Mech Eng. 2019;7(1):1-10.
[18] Hoonpong P, Promthaisong, Skullong S. Experimental study of thermal performance in a tubular heat exchanger using inclined perforated vortex rings. J Res Appl Mech Eng. 2020;8(2):148-57.
[19] Lamlerd B, Bubphachot B, Chompookham T. Experimental investigation of heat transfer characteristics of steam generator with circular-ring turbulators. Case Stud Therm Eng. 2023;41:102549.
[20] Pimsarn M, Samruaisin P, Thianpong C, Ruengpayungsak K, Eiamsa-ard P, Chamoli S, et al. Performance of a heat exchanger with compound inclined circular-rings and twisted tapes. Case Stud Therm Eng. 2022;37:102285.
[21] Promvonge P, Skullong S. Thermohydraulic performance and entropy generation in heat exchanger tube with louvered winglet tapes. Int J Therm Sci. 2022;181:107733.
[22] Jayranaiwachira N, Promvonge P, Thianpong C, Skullog S. Entropy generation and thermal performance of tubular heat exchanger fitted with louvered corner-curved V-baffles. Int J Heat Mass Transf. 2023;201(1):123638.
[23] Siriwan N, Bubphachot B, Eiamsa-ard S, Wongcharee K, Chompookham T, Promthaisong P. 3D Simulation on turbulent flow and heat transfer behaviors in a five-start corrugated tube: Effect of depth ratio and tube modification. Eng Appl Sci Res. 2021;48(6):694-703.
[24] Fagr MH, Rishak QA, Mushatet KS. Performance evaluation of the characteristics of flow and heat transfer in a tube equipped with twisted tapes of new configurations. Int J Therm Sci. 2020;153:106323.
[25] Altun AH, Nacak H, Canli E. Effects of trapezoidal and twisted trapezoidal tapes on turbulent heat transfer in tubes. Appl Therm Eng. 2022;211:118386.
[26] Samutpraphut B, Eiamsa-ard S, Chuwattanakul V, Thianpong C, Maruyama N, Hirota M. Influence of sawtooth twisted tape on thermal enhancement of heat exchanger tube. Energy Rep. 2023;9(S1):696-703.
[27] Altun AH, Ors S, Dogan S. Investigation of effects on turbulent heat transfer of twisted wavy tape elements in the tube. Int J Therm Sci. 2023;185:108068.
[28] Bahuguna R, Mer KKS, Kumar M, Chamoli S. Thermal performance of a circular tube embedded with TBVG inserts: an experimental study. J Therm Anal Calorim. 2022;147:11373-89.
[29] Patankar SV. Numerical heat transfer and fluid flow. New York: McGraw–Hill; 1980.
[30] ANSYS Inc. ANSYS Fluent Theory Guide, 18th version. Canonsburg: SAS IP Inc.; 2017.
[31] Incropera F, Dewitt PD, Bergman TL, Lavine AS. Introduction to heat transfer. 6th ed. New Jersey: John Wiley & Sons; 2006.